Cell Reports, Volume *30*

Supplemental Information

hnRNPDL Phase Separation Is Regulated by Alternative Splicing and Disease-Causing Mutations Accelerate Its Aggregation

Cristina Batlle, Peiguo Yang, Maura Coughlin, James Messing, Mireia Pesarrodona, Elzbieta Szulc, Xavier Salvatella, Hong Joo Kim, J. Paul Taylor, and Salvador Ventura

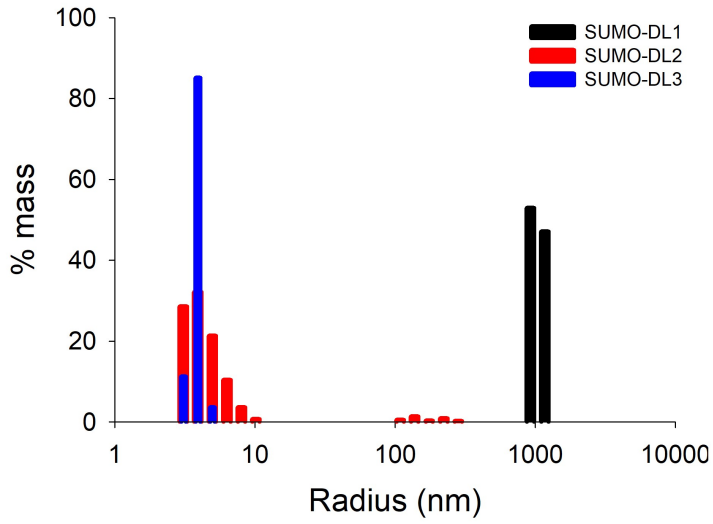

Figure S1. Dynamic Light Scattering of hnRNPDL isoforms. Related to Figure 1.

Dynamic Light Scattering (DLS) radius (nm) versus % of mass of hnRNPDL isoforms 1, 2 and 3 (SUMO-DL1, DL2 and DL3 fusions) at 50 μM in 50 mM HEPES pH 7.5 and 150 mM NaCl, in the absence of crowding agents.

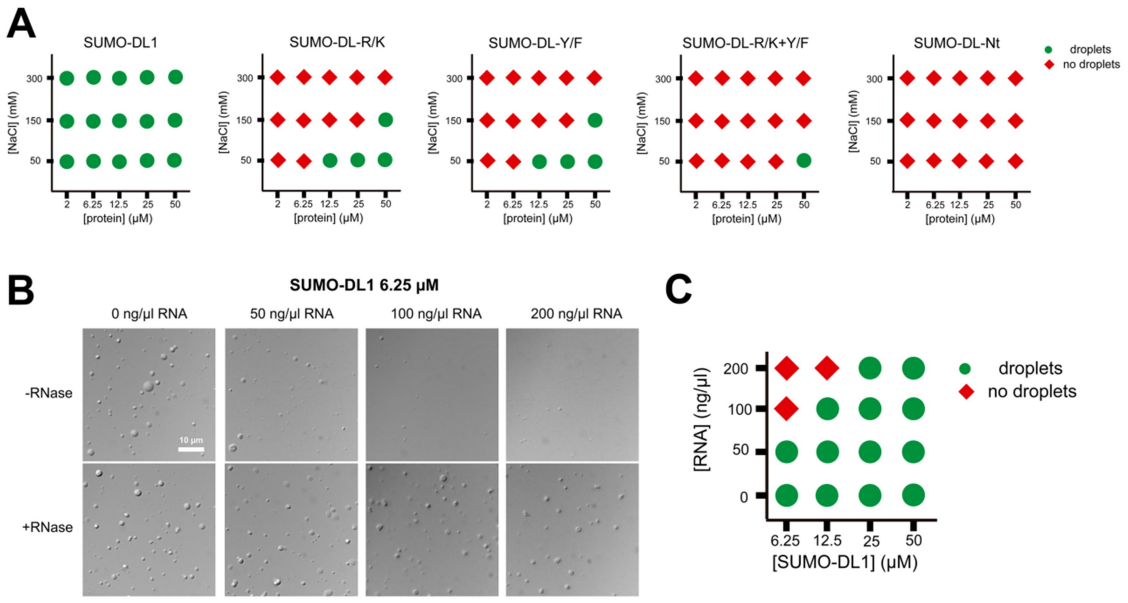

Figure S2. Liquid-liquid phase separation diagram of hnRNPDL isoform 1 after mutation or RNA addition. Related to Figure 2 and Figure 3.

A) LLPS diagram of hnRNPDL isoform 1 (SUMO-DL1) and the four hnRNPDL variants: SUMO-DL-R/K, SUMO-DL-Y/F, SUMO-DL-R/K+Y/F and SUMO-DL-Nt, in the absence of crowding agents. Green circles indicate positive and red diamonds indicate negative for the appearance of droplets at the indicated NaCl/protein concentration combinations. B) SUMO-hnRNPDL isoform 1 (DL1) LLPS at 6.25 μM (366 ng/μl) in the presence of different concentrations of total RNA with or without 5 ng/μl RNase in 50 mM HEPES pH 7.5 and 150 mM NaCl. C) LLPS diagram of DL1 as a function of protein and RNA concentration in 50 mM HEPES pH 7.5 and 150 mM Nacl. Green circles indicate positive and red diamonds indicate negative for the appearance of droplets at the indicated RNA/protein concentration combinations.

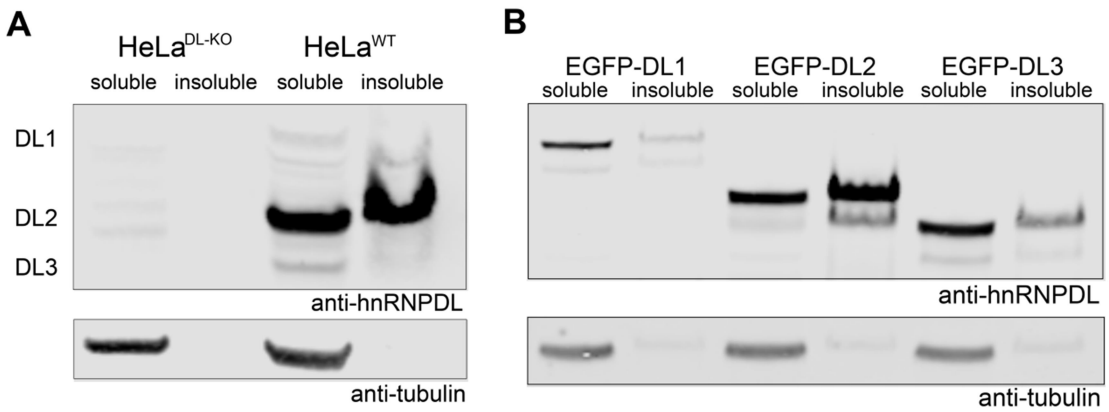

Figure S3. Endogenous or individual isoforms hnRNPDL solubility analysis after expression in HeLa WT or hnRNPDL KO cells. Related to Figure 3 and Figure 5.

A) Cell extracts of HeLa hnRNPDL KO ($HeLa^{DL\text{-}KO}$) and HeLa WT were processed for soluble examination by Western Blot using an antibody against hnRNPDL protein. Tubulin was blotted as a loading control. B) Cell extracts of $HeLa^{DL\text{-}KO}$ after EGFP-tagged hnRNPDL isoform 1, 2 or 3 (EGFP-DL1, DL2 and DL3) expression were fractionated and the soluble and insoluble fractions analyzed by Western Blot using an antibody against hnRNPDL protein. Tubulin was blotted as a loading control.

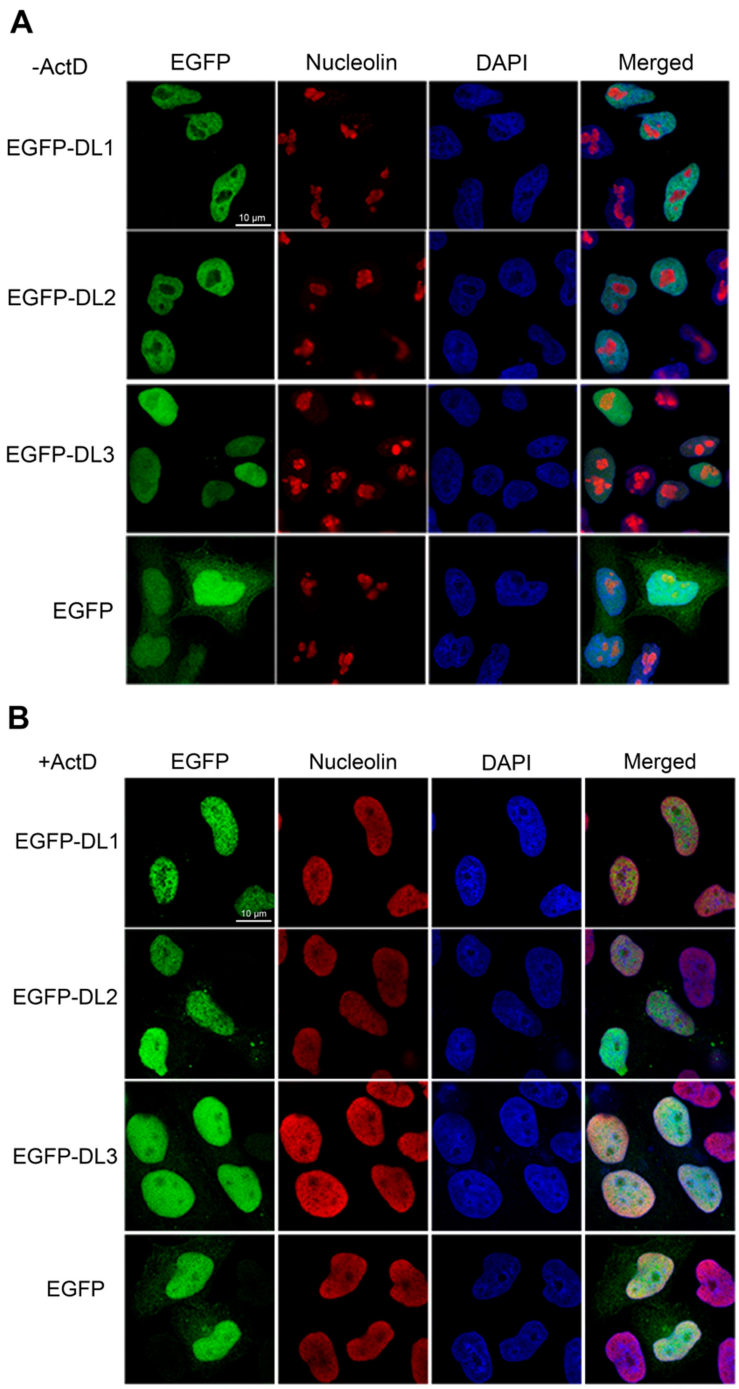

Figure S4. HnRNPDL isoforms localization in HeLa$^{DL\text{-}KO}$ cells. Related to Figure 3 and Figure 4. Cellular localization by immunofluorescence of EGFP-hnRNPDL isoform 1, 2 and 3 (DL1, DL2, DL3) and unfused EGFP after expression in HeLa$^{DL\text{-}KO}$ cells in the absence (A) or the presence (B) of actinomycin D. Cells were stained with nucleolin antibody (red) as nucleolus marker and DAPI (blue) as nuclear marker.

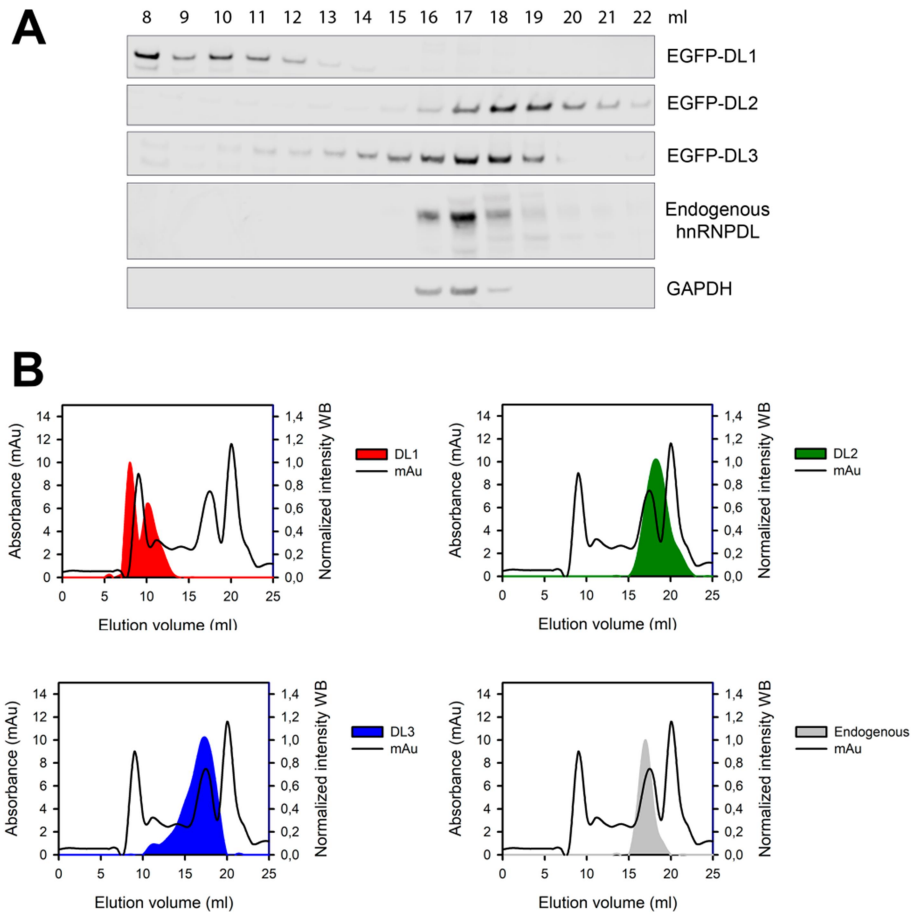

Figure S5. Elution pattern of cellular hnRNPDL isoforms. Related to Figure 3.
A) Cell extracts of HeLa$^{DL\text{-}KO}$ cells after EGFP-tagged hnRNPDL isoform 1, 2 or 3 (EGFP-DL1, DL2 and DL3) expression as well as HeLa WT cells were fractionated by size exclusion chromatography (SEC) and fractions at different elution volumes (ml) were analyzed by Western Blot (WB) using an antibody against hnRNPDL protein. GAPDH was blotted as a loading and molecular weight control. B) WB intensities of EGFP-DL1, DL2 and DL3 and endogenous hnRNPDL were plotted on top of a representative SEC graph of HeLa cells extracts.

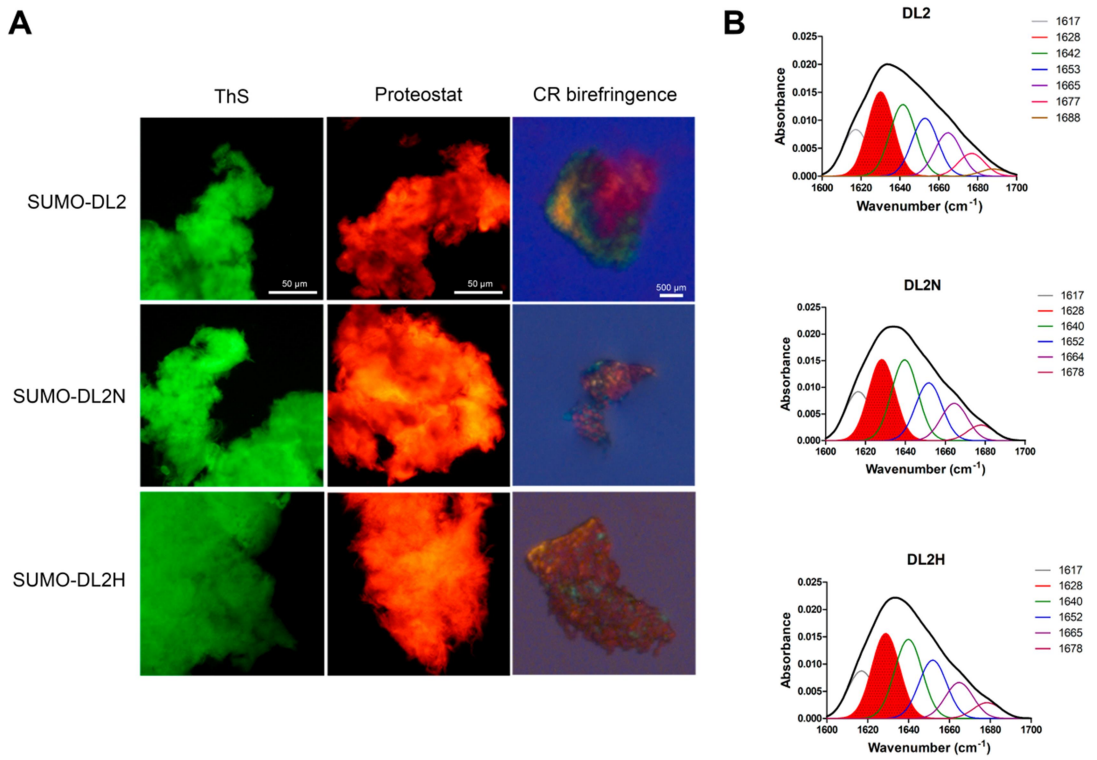

Figure S6. Amyloid properties of hnRNPDL isoform 2 and disease-causing mutations. Related to Figure 5 and 6.

A) Thioflavin-S (ThS) staining, Proteostat® staining and Congo Red (CR) birefringence of 4 days incubated 50 µM SUMO-hnRNPDL isoform 2 (DL2) and the disease-causing mutations D259N and D259H (DL2N and DL2H) in 50 mM HEPES pH 7.5 and 150 mM NaCl. B) DL2, DL2N and DL2H FTIR absorbance spectrum in the amide I region after aggregation at 50 µM in 50 mM HEPES pH 7.5 and 150 mM NaCl. The black line corresponds to the original absorbance spectrum and the red dotted area indicates the contribution of the intermolecular β-sheet signal to the total area upon Gaussian deconvolution. Aggregation was conducted at 37ºC and 600 rpm in both A and B.

Figure S7. HnRNPDL exon 6 alignment in vertebrates. Related to Figure 6.

hnRNPDL exon 6 alignment between human, mouse, rat, chicken, xenopus and zebrafish organisms using Clustal Omega. Asp disease-causing mutation is in red.

Rosetta energy (kcal/mol)	DL2	DL2N	DL2H
Average six hexapeptides	-19.4	-20.7	-21.2
Maximum scored hexapeptide GGYDYT	-20.7	-22.4	-22.2

Table S1. ZipperDB analysis of hnRNPDL isoform 2 and disease-causing mutations. Related to Figure 6.

ZipperDB analysis of hnRNPDL isoform 2 and the disease-causing mutations D259N and D259H (position 378 in hnRNPDL isoform 1) (DL2N and DL2H). The average of the Rosetta energy for the 6 possible hexapeptides containing the Asp mutated residue and the hexapeptide with the highest score are presented in the table.

SUMO-DL2		SUMO-DL2N		SUMO-DL2H	
Peak	**% area**	**Peak**	**% area**	**Peak**	**% area**
1617	13.99	1617	15.24	1617	14.78
1628	25.23	1628	25.23	1628	26.39
1642	21.45	1640	25.12	1640	24.59
1653	17.36	1652	17.98	1652	18.13
1665	13.00	1664	11.60	1665	11.19
1677	6.82	1678	4.83	1678	4.93
1688	2.15				

Table S2. Secondary structure content of hnRNPDL isoform 2 and disease-causing mutations aggregates. Related to Figure 6 and Figure S6.

Position and relative area of spectral components in the amide I region of the FTIR absorbance spectrum for the aggregated hnRNPDL isoform 2 and the disease-causing mutations D259N and D259H (DL2N and DL2H).

Bacteria primers	**Primers 5' → 3'**
SUMO-DL1_F	CGCGAACAGATTGGAGGTGAAGTCCCGCCGCGTCTG
SUMO-DL1_R	GTGGCGGCCGCTCTATTAGTACGGTTGATAATTGTT
SUMO-DL2_F	GAAGACATGAACGAATACAGC
SUMO-DL2_R	ACCTCCAATCTGTTCGCGGTG
SUMO-DL3_F	CAAAGCACGTACGGTAAAGCAAG
SUMO-DL3_R	CTGACCACGGCCGCGACCACG
SUMO-DL2N_F	AACTACACCGGCTATAACTAC
SUMO-DL2N_R	ATAACCGCCGTAACCGCTATAG
SUMO-DL2H_F	CACTACACCGGCTATAACTAC
SUMO-DL2H_R	ATAACCGCCGTAACCGCTATAG
SUMO-DL1R/K_F	GAAGACATGAACGAATACAGC
SUMO-DL1R/K_R	ACCTCCAATCTGTTCGCGGTG
SUMO-DL1-Y/F_F	CAAAGCACGTACGGTAAAGC
SUMO-DL1-Y/F_R	CTGACCACGGCCGCGACCACGGGT
SUMO-DL-Nt_F	TAATAGAGCGGCCGCCACCGCT
SUMO-DL-Nt_R	CATCGTGACGCTCGAATCTG
Mammalian primers	**Primers 5' → 3'**
EGFP-C3-DL1_F	GTACTCAGATCTCGAGCTCAAGCTTATGGAGGTCCCGCCCAGGCTTTC
EGFP-C3-DL1_R	CAGTTATCTAGATCCGGTGGATCCTTAGTATGGCTGGTAATTGTTT
EGFP-C3-DL2_F	GAGGATATGAACGAGTACAGC
EGFP-C3-DL2_R	AAGCTTGAGCTCGAGATCTGAG
EGFP-C3-DL3_F	CAGAGCACTTATGGCAAGGCATC
EGFP-C3-DL3_R	CTGACCTCGGCCACGACCCCTC
EGFP-C3-DL2N_F	AATTATACTGGGTATAACTATG
EGFP-C3-DL2N_R	ATATCCGCCATAGCCACTATAG
EGFP-C3-DL2H_F	CATTATACTGGGTATAACTATG
EGFP-C3-DL2H_R	ATATCCGCCATAGCCACTATAG
DNA fragments	**Primers 5' → 3'**
DNA fragment R/K	CACCGCGAACAGATTGGAGGTGAAGTCCCGCCGAAACTGAGTCATGTCCCGC CGCCGCTGTTCCCGAGCGCACCGGCAACCCTGGCAAGCAAGAGCCTGTCGCA CTGGAAGCCGAAACCGCCGAAACAGCTGGCACCGCTGCTGCCGTCCCTGGCC CCGAGCTCTGCAAAGCAGGGCGCTAAGAAAGCGCAAAAGCATGTTACCGCAC AGCAACCGAGTAAACTGGCAGGCGGTGCGGCCATTAAAGGCGGTAAGAAGAA GAAACCGGACCTGTTTAAGAAACATTTCAAAAGTTCCTCAATCCAGAAGAGC GCAGCTGCGGCCGCAGCTACCAAGACGGCTAAACAGCACCCGCCGGCAGATT CGAGCGTCACGATGGAAGACATGAACGAATACAGC
DNA fragment Y/F	ACCCGTGGTCGCGGCCGTGGTCAGGGCCAAAACTGGAACCAGGGTTTCAACA ACTTCTTCGATCAAGGTTTCGGCAACTTCAATTCGGCGTTTGGCGGTGATCA GAACTTTAGCGGTTTCGGCGGTTTTGACTTCACCGGCTTTAACTTCGGTAAT TTTGGTTTCGGCCAGGGTTTTGCCGATTTCTCGGGCCAGCAAAGCACGTACG GTAAAGC

Table S3. List of the primers used in this study. Related to STAR Methods.

The source of all the primers is from this study and there is no identifier.